CrossMark

HEAD AND NECK

Diagnostic and prognostic value of 18F-FDG PET, CT, and MRI in perineural spread of head and neck malignancies

Laurent Dercle[1,2,3] · Dana Hartl[4] · Laura Rozenblum-Beddok[1] ·
Fatima-Zohra Mokrane[5,6] · Romain-David Seban[1] · Randy Yeh[3] · François Bidault[1] ·
Samy Ammari[1]

Abstract

Objectives We assessed whether quantitative imaging biomarkers derived from fluorodeoxyglucose-positron emission tomography (18F-FDG PET) could be extracted from perineural spread (PNS) in head and neck malignancies (HNM) to improve patient risk stratification.

Methods A case–control exploratory study (1:2 ratio) enrolled 81 patients with FDG-avid HNM. The case-group comprised 28 patients with documented PNS (reference: expert consensus), including 14 squamous cell carcinomas (SCC). Imaging biomarkers were extracted from the PNS on 18F-FDG PET, CT-scan, and MRI. The control-group enrolled 53 SCCs. The Cox proportional-hazards regression model explored the association with overall survival by univariate and multivariate analyses.

Results The rate of PNS detection by 18F-FDG PET was 100% in the case-group. Quantitative imaging biomarkers were not associated with the presence of sensory (*p*>0.20) or motor (*p*>0.10) symptoms. In SCC patients (case: 14; control: 53), PNS was associated with a hazard ratio of death of 5.5 (95%CI: 1.4:20.9) by multivariate analysis. Increased cranial nerve SUV_{max} was significantly associated with poorer overall survival by univariate analysis (*p*=0.001).

Conclusions Our pilot study showed the feasibility of extracting 18F-FDG PET biomarkers from PNS in FDG-avid HNM. Our results encourage the development of new PET/CT- or PET/MRI-guided management strategies in further prospective studies.

Key Points
• *18F-FDG PET/CT detects PNS in FDG-avid HNM.*
• *PNS metabolism is more heterogeneous than healthy tissue.*
• *PNS diagnosis is crucial: most patients were asymptomatic, N0 and M0.*
• *PNS diagnosis is associated with poorer overall survival in SCC.*
• *PET/CT- or PET/MRI-guided management strategies should be evaluated.*

Keywords Perineural spread · Perineural extension · Head and neck cancer · 18F-FDG PET · MRI

François Bidault and Samy Ammari Contributed equally to this work

✉ Laurent Dercle
laurent.dercle@gmail.com

✉ François Bidault

✉ Samy Ammari

1 Département d'imagerie médicale, Institut Gustave-Roussy, 94805 Villejuif, France

2 UMR1015, Institut Gustave Roussy, 94800 Villejuif, France

3 Department of Radiology, New York Presbyterian Hospital, Columbia University Medical Center, New York, NY 10039, USA

4 Département d'oto-rhino-laryngologie, Institut Gustave-Roussy, 94805 Villejuif, France

5 Radiology department, Rangueil University Hospital, 1 avenue du Professeur Jean Poulhes. 31059 CEDEX, Toulouse, France

6 French National Center for Scientific Research, AMIS Laboratory: University of Toulouse, UMR 5288, 37 allées Jules Guesde, 31073 Toulouse, France

Abbreviations

PNS	Perineural spread
SUV	Standardised uptake value
HISUV	Heterogeneity index of the standardised uptake value
V[1]	Ophthalmic branch of the trigeminal nerve
V[2]	Maxillary branch of the trigeminal nerve

V^3	Mandibular branch of the trigeminal nerve
VII	Facial nerve

Introduction

Head and neck malignancies (HNM) can extend along neurovascular routes, leading to greater difficulty in locoregional control of the disease. Perineural spread (PNS) is associated with worse outcome, including poorer prognosis, lower survival rate, and increased rates of local recurrence and distant metastasis [1]. The early detection of PNS thus has a tremendous impact on patient management, with implications for risk stratification, staging, treatment planning, and follow-up.

Medical imaging guides challenging treatment decisions, with the goal of striking the optimal balance between satisfactory oncological and functional results. Medical imaging then plays a key role in assessing the efficacy of treatment strategies. There is growing interest in the power of big data from medical imaging to fill knowledge gaps and identify alternative metrics that can predict patient outcome at an early stage. In that context, FDG PET provides early prognostic and predictive biomarkers that outperform CT and MRI [2–4].

At our tertiary reference centre, we observed that PNS in HNM was rarely reported on 18F-FDG PET/CT, compared to direct tumour extension pathways and lymphatic dissemination [1]. Additionally, we noted that PNS was the least documented route of locoregional spread in the 18F-FDG PET/CT literature, with only a few case reports [5–10]. This prompted us to investigate whether intrinsic limiting factors of PET were responsible for poor sensitivity in the detection of cranial nerve involvement. One hypothesis is that the low rate of PNS detection by 18F-FDG PET stems from its intrinsic limitations: limited spatial resolution and the high physiological FDG uptake of the nearby brain.

The current consensus is that there are no significant differences between PET/MRI and PET/CT in HNM, although there is a trend towards higher accuracy for resectability [11–13]. However, patients with perineural spread represent a very specific population, requiring specific treatment strategies that are never systematically analysed in PET studies, thus creating a knowledge gap in the current literature. Theoretically, patients with PNS might benefit from hybrid modalities such as 18F-FDG PET/CT or PET/MRI.

This paper constitutes a preliminary pilot study of the extraction of PET biomarkers from PNS, with the intent that these data could enable the development of new PET-guided management strategies. The primary objective of the study was to determine the effectiveness of 18F-FDG PET for the detection of PNS using a case–control design. The secondary objective was to evaluate whether quantitative imaging biomarkers derived from metabolic activity (18F-FDG PET) and anatomical characteristics (contrast-enhanced CT scan and MRI) of the PNS could improve risk stratification of patients for overall survival.

Patients and methods

Patient selection

This case–control study (1:2 ratio) enrolled 81 patients with FDG-avid HNM during the period from May 2009 to July 2017 in a comprehensive cancer centre. The study included consecutive patients reviewed by the tumour board for initial management or locoregional recurrence of PNS of HNM. The reference standard for the diagnosis of PNS was MRI and tumour board conclusion. PNS was confirmed by analysis of histology on surgery (12 patients) or by typical tumour evolution ($n = 28$) during follow-up. The mean (SD) follow-up was 13 (15) months in the case group and 12 (16) months in the control group. 18F-FDG PET evaluation was performed within a mean (SD) of 21 (24) days from the MRI in the case group and 21 (20) days in the control group. The need for ethical approval was waived by the local research ethics committee.

Imaging protocols

MRI acquisitions (transverse, sagittal, coronal views) were performed with a 1.5-Tesla unit (Signa Excite HD, GE Healthcare, Milwaukee, WI, USA) using T2-weighted sequences and T1-weighted sequences with and without gadolinium chelate injection and fat signal suppression. 18F-FDG PET/CT acquisitions and reconstructions were performed according to the European Association of Nuclear Medicine/European Society of Cardiology (EANM/ESC) guidelines for PET tumour imaging (intravenously injected FDG activity: 3-4 MBq/kg). Images were acquired on a GE Discovery 690 unit (GE Medical Systems, Waukesha, WI, USA) with lutetium-yttrium oxyorthosilicate (LYSO)-based detectors. Whole-body acquisitions (2 min per bed) were obtained 60 min post-injection from head to mid-thigh, including dedicated head and neck reconstructions (3 min per bed), for detection of small lymph node metastases and decreased risk of motion artefacts [14]. Unenhanced CT scans allowed for attenuation correction. A fully 3D time-of-flight iterative reconstruction scheme (GE VUE Point FX [VPFX]; GE Healthcare) was used (ordered subset expectation maximization [OSEM] algorithm with scatter, random coincidence, dead time, attenuation, and normalisation corrections). The isotropic voxel size was 3 mm (matrix: 256×256).

Extraction of quantitative imaging biomarkers

Magnetic resonance imaging PNS was recorded as positive if two major signs of cranial nerve involvement were registered [15–18] using a three-plane axis (Fig. 1). The major signs of cranial nerve involvement were as follows [6; 7]: (i) topography of the abnormality typically along or within the distributions of a cranial nerve (focal, linear, or curvilinear) and in close proximity to the primary lesion or the site of recurrence; (ii) enlargement of the cranial nerve in comparison to supposed healthy contralateral nerve and/or contrast enhancement asymmetry. The major signs of foramina extent included the following: (i) the abnormality concerned a foramen involved by a cranial nerve in contact with the tumour (e.g. foramen ovale and cranial nerve V^3, foramen rotundum and cranial nerve V^2); (ii) enlarged foramen and/or bone erosion were present. Minor indirect signs included (i) absence/replacement of normal juxtaforaminal fat (in the skull base and in the pterygopalatine fossa) on MRI identified by decreased T1 signal intensity on a T1-weighted sequence without gadolinium chelate injection; and (ii) presence of acute or chronic nerve dysfunction (muscular changes due to denervation) which was non-specific. Acute nerve dysfunction was characterised by increased T2 signal, decreased T1 signal, increased enhancement of the muscle, and increased muscle volume (e.g. masticatory space and cranial nerve V^3). Muscular atrophy due to a fatty involution of the muscle was recorded as an indirect sign of chronic nerve dysfunction (increased T1 and T2 signal).

18F-FDG PET/CT Metrics were calculated within the primary head and neck tumour, the PNS, and the brain (contralateral healthy cortex of the cerebellum) using PET VCAR (Volume Computer Assisted Reading; GE Healthcare). The metabolic tumour volume (MTV) was obtained using a segmented volume based on a 42% threshold of SUV_{max}. The standardised uptake value (SUV), SUV_{max}, and SUV_{mean} were extracted within this volume of interest. We computed the SUV heterogeneity index (HISUV) as follows: $HISUV = SUV_{max} / SUV_{mean}$ [19].

Statistical analysis

Data were presented as frequency and percentages for qualitative variables and as mean with standard deviation for continuous variables. The 95% confidence intervals (95% CI) of binary variables were calculated assuming a binomial distribution. Calculated data with p values < 0.05 were considered statistically significant. Analysis of variance (ANOVA) was conducted to compare the distribution of the variables between subgroups, assuming a normal distribution. The diagnostic ability of quantitative imaging biomarkers to detect a malignant process was calculated using a binary classification system (normal tissue vs. malignant process) and a receiver
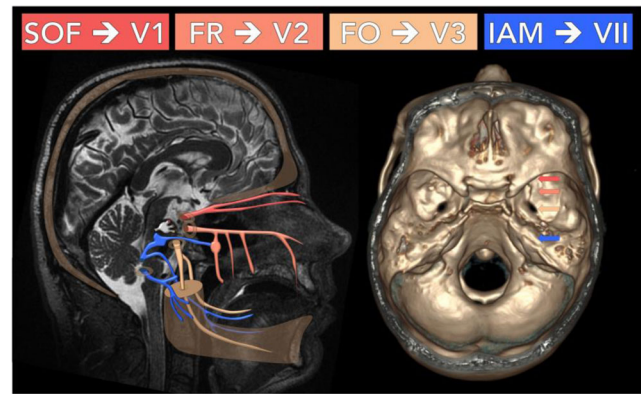

Fig. 1 Most frequent sites of perineural spread. The most frequently involved cranial nerves are V1, V2, V3, and VII, which pass through the superior orbital fissure (SOF), the foramen rotundum (FR), the foramen ovale (FO), and the internal acoustic meatus (IAM), respectively

operating characteristic (AUC) curve. A Cox proportional hazards regression model was used for studying the dependency of overall survival time on predictor variables in the population of patients with squamous cell carcinoma (SCC; case group: 14; control group: 53). First, we incorporated the presence of PNS into the TNM Classification of Malignant Tumours (TNM) model (i.e. the current reference standard for tumour staging and risk stratification) to determine whether it added information by multivariate analysis. We then determined the association between quantitative imaging biomarkers extracted from PNS and overall survival by univariate analysis. We computed the association with overall survival in the entire cohort of SCC patients using Kaplan-Meier analysis and divided our cohort into two groups: case and control. All statistical analyses were performed using SPSS version 24.0 software (IBM Corp., Armonk, NY, USA).

Results

Patient characteristics

Eighty-one patients were included: 28 patients in the case group and 53 in the control group. In the case group, the primary tumour histological subtypes were SCC (50%), adenoid cystic carcinoma (14%), and sarcoma (11%). Other subtypes included odontogenic tumour, esthesioneuroblastoma, and embryonal rhabdomyosarcoma. Table 1 provides a summary of patient characteristics.

Detection of PNS by 18F-FDG PET

Overall characteristics See Table 2.

Detection rate 18F-FDG PET/CT detected PNS in all patients in the case group ($n = 28/28$), with no false-positive results in

Table 1 Main patient characteristics

	Control group	PNS case group		
	SCC	Overall	SCC	Non SCC
PATIENTS				
No.	53	28	14	14
Age (years)	61 ± 20	52 ± 17	53 ± 12	52 ± 22
Male gender (%)	81	86	86	86
Follow-up after reference 18F-FDG PET/CT				
Follow-up (months)	12 ± 16	13 ± 15	8 ± 8	19 ± 19
Death (%)	23	39	64	14
Management (%)				
Chemotherapy	87	82	93	71
External beam radiation therapy	94	89	100	79
Surgery	33	32	36	29
TUMOUR				
TNM at staging (%)				
T3 or T4	46	86	75	100
N1 or more	83	38	38	36
M1	4	9	0	18
Pathology (%)				
Adenoid cystic carcinoma	0	14	0	29
Squamous cell carcinoma	100	50	100	0
Sarcoma	0	11	0	21
Other	0	25	0	50
Tumour location (%)				
Midface location	N/A	89	86	93
Tongue	17	14	29	0
Maxillary sinus	0	18	21	14
Nasopharynx	4	32	21	43
Parotid gland	0	4	0	7
Ethmoid, skull base, sphenoid sinus	0	11	0	21
Tonsil, soft palate	60	11	14	7
Skin (face, vertex, lips)	0	11	14	7
Other	19	0	0	0
PERINEURAL SPREAD				
PNS symptoms (%)				
Sensory symptoms	N/A	48	62	36
Motor symptoms	N/A	41	46	36
PNS in medical history				
Delay since first diagnosis of HNM (months)	N/A	20 ± 30	22 ± 28	18 ± 33
PNS diagnosed at staging (%)	N/A	57	21	93
PNS diagnosed after a recurrence (%)	N/A	43	79	7

Values are expressed as mean ± SD or as a percentage

the control group ($n = 0/53$). Consequently, the detection rate (95% confidence interval) was 100% (88:100). Figure 2 shows that the SUV_{max} was greater than 10 in most patients despite the limited spatial resolution of PET.

Typical topography of PNS We observed a typical distribution of PNS along specific cranial nerves V^3 (61%), V^2 (43%), V^1 (7%), and VII (4%), with a total of 35 instances of PNS detected among the 28 patients.

Table 2　Main imaging features in patients with PNS on 18F-FDG PET, CT scan, and MRI

	Overall	SCC	Non-SCC
No.	28	14	14
Delay between PET and MRI (days)	21±25	16±20	26±29
PRIMARY TUMOUR			
Metabolism			
SUVmax	19±11	20±13	18±9
SUVmean	14±8	15±10	13±6
HISUV	1.5±0.2	1.5±0.2	1.5±0.2
Morphology			
1D-Maximum diameter (cm)	4±2	4±2	4±1
2D-Product of the maximum diameters (cm^2)	16±12	19±15	13±7
3D-Product of the maximum diameters (cm^3)	57±69	76±57	37±35
CRANIAL NERVE			
Number of cranial nerve involved	35	16	19
Site			
I	4%	0%	7%
V^1	7%	14%	0%
V^2	43%	29%	57%
V^3	61%	57%	64%
PPF	4%	7%	0%
VII	4%	0%	7%
IX, X, XI or XII	4%	7%	0%
Metabolism			
SUVmax	18±11	20±13	16±8
SUVmean	13±7	14±9	11±6
HISUV	1.5±0.1	1.6±0.1	1.5±0.2
Morphology			
Contrast enhancement of the nerve (MRI)	100%	100%	100%
Maximum diameter (mm)			
PNS	10±5	8±3	11±6
Normal contralateral cranial nerve	2.5±1.2	2.4±1.0	2.6±1.5
Ratio	4.5±3.2	3.9±2.0	5.1±4.1
Twofold enlargement on CT	86%	71%	100%
FORAMEN			
Minimum diameter (mm)			
Foramen involved by cranial nerve	8±4	7±3	9±5
Normal contralateral foramen	3.1±1.2	3.3±1.4	3.0±1.0
Ratio	2.7±1.6	2.4±1.5	3.0±1.7
Twofold enlargement on CT	68%	50%	86%
Aggressive osteolysis	18%	21%	14%
BRAIN			
SUVmax	15±6	14±5	16±7
SUVmean	14±5	12±3	16±5
HISUV	1.2±0.1	1.2±0.1	1.2±0.1

Values are expressed as mean ± SD or as a percentage

Increased FDG uptake within PNS The average maximum metabolism within the primary tumour site of HNM (SUV$_{max}$: 19 ± 11) and PNS (SUV$_{max}$: 18 ± 11) did not differ significantly from the physiological healthy cortex brain uptake (SUV$_{max}$: 15 ± 6) according to ANOVA ($p = 0.30$ and $p = 0.37$, respectively). Consequently, there was no significant threshold
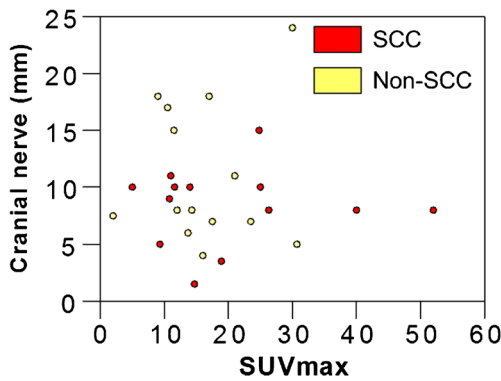
Fig. 2 SUV_{max} and cranial nerve size in PNS of both SCC and non-SCC patients. Despite the limited spatial resolution of PET, the FDG uptake was significantly increased in all PNS

enabling differentiation of the tumour tissue from the brain tissue: SUV_{max} (AUC [95% CI]: 0.53 [0.36-0.71], $p = 0.69$) and SUV_{mean} (AUC [95% CI]: 0.37 [0.20-0.54], $p = 0.14$, assuming that the higher SUV_{mean} should be associated with the malignant process). We concluded that healthy brain physiological metabolism could potentially mask an increased FDG uptake within PNS, although this was not observed in our series.

Heterogeneity of FDG uptake The HISUV (mean $\pm$ SD) was 1.5 ± 0.2, 1.5 ± 0.1, and 1.2 ± 0.1 within the primary tumour, the PNS, and the brain, respectively. The HISUV of the PNS was similar to that of the primary tumour and 30% higher than that of healthy brain tissue in all cases (ANOVA, $p < 0.001$). HISUV > 1.3 achieved 95% sensitivity and 100% specificity for differentiating between a cranial nerve invaded by PNS and healthy cortex brain tissue (AUC [95% CI]: 0.98 [0.95-1.00], $p < 0.001$).

Risk stratification for the prediction of overall survival

We compared the overall survival of patients with SCC between those in the case ($n = 14$) and control groups ($n = 50$). Table 1 shows patient characteristics. On average, patients in the case group tended to be younger (53 vs. 61 years of age) and were less frequently N1 (38% vs. 83%) or M1 (0% vs. 4%) than the control group. The management was comparable.

Kaplan-Meier analysis (Fig. 3) showed significantly poorer overall survival in the case group (Kaplan-Meier analysis: $p = 0.003$).

In the multivariate Cox proportional hazards regression model (Table 3), the presence of PNS was associated with a hazard ratio of 5.5 (1.4:20.9; $p = 0.013$). Univariate Cox regression analysis (Table 4) showed that the ratio of cranial nerve SUV_{max} displayed the strongest association with overall survival ($p = 0.001$). This ratio compares the metabolism in the PNS with the metabolism in the contralateral cranial nerve.
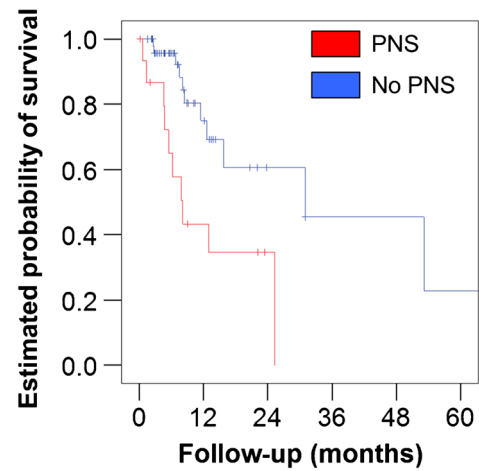
Hazard Ratio 3.5 (95CI: 1.4 : 8.7), P=0.006

Fig. 3 Kaplan-Meier analysis showed poorer cumulative overall survival (p=0.003) in SCC patients with PNS

Therefore, the ratio is 1 in the control group, because both cranial nerves are normal.

Association with clinical symptoms

Quantitative imaging biomarkers were not associated with the presence of clinical sensory or motor symptoms. The ANOVA showed no significant differences between patients with sensory symptoms and asymptomatic patients with regard to SUV_{max} ($p = 0.80$), SUV_{mean} ($p = 0.95$), HISUV ($p = 0.20$), or the ratio of nerve enlargement ($p = 0.27$). In addition, ANOVA showed no significant differences between patients with motor symptoms and asymptomatic patients with regard to SUV_{max} ($p = 0.38$), SUV_{mean} ($p = 0.37$), HISUV ($p = 0.86$), or the ratio of nerve enlargement ($p = 0.10$).

Discussion

Our preliminary pilot study confirmed the feasibility of extracting 18F-FDG PET biomarkers from PNS in FDG-

Table 3 Cox proportional hazards regression model for the multivariate analysis of overall survival data in squamous cell carcinoma patients

Variable	Univariate analysis		Multivariate analysis	
	Hazard ratio	*p*-value	Hazard ratio	*p*-value
Perineural spread	3.5 (1.4 : 8.7)	0.01	5.5 (1.4 : 20.9)	0.01
$\geq$ T3	1.8 (0.7 : 4.6)	0.22	1.0 (0.3 : 3.3)	0.94
$\geq$ N1	0.7 (0.3 : 1.6)	0.39	1.7 (0.5 : 5.9)	0.42
$\geq$ M1	3.3 (0.4 : 25.3)	0.33	5.7 (0.7 : 50.5)	0.11

Table 4 Cox proportional hazards regression model for the univariate analysis of overall survival data in squamous cell carcinoma patients

Variable	Hazard ratio	*p*-value
Ratio of cranial nerve diameter	1.22 (1.00 : 1.50)	0.05
Ratio of foramen diameter	1.21 (0.78 : 1.87)	0.40
Ratio of cranial nerve SUVmax	1.05 (1.02 : 1.08)	0.001
Ratio of cranial nerve HISUV	11.05 (2.29 : 53.39)	0.003

avid HNM. Our results should encourage the development of new PET/CT or PET/MRI-guided management strategies in further prospective studies.

In a large series including 28 patients with PNS (Figs. 4, 5, 6), we reported 100% detection of PNS by 18F-FDG PET and described five direct or indirect imaging signs: (i) increased FDG uptake; (ii) heterogeneous glucose consumption; (iii) typical topography along/within cranial nerves V^3, V^2, V^1, and VII; (iv) cranial nerve enlargement; and (v) foramen enlargement. These excellent results are the consequence of a very sensitive reading by a pair of specialists trained in the detection of PNS in FDG-avid malignancies. Our findings suggest that the underdiagnosis of PNS using 18F-FDG PET in clinical routine should not be attributed solely to technical limitations, such as the limited spatial resolution of PET and the physiological FDG uptake of the nearby brain.

Nonetheless, the aim of our report is not to suggest that 18F-FDG PET might replace MRI for PNS detection. MRI is the reference standard [18, 20–22] and achieves 95% sensitivity in detecting PNS and 63% sensitivity for accurate mapping of the complete PNS [23], due to its multiplanar capability and superior soft tissue contrast [16]. In comparison, CT is superior in detecting indirect signs of nerve enlargement, such as foramina enlargement and foramina destruction in the bony skull base [16]. Indeed, our opinion is that PET and MRI could be combined, and that contrast-enhanced PET/MRI will outperform PET/CT if PNS is anticipated, as suggested by a study in which PNS was detected in three of 44 primary tumours (7%) [13].

The detection of PNS is clinically significant, since PNS is frequently asymptomatic at the time of initial staging and is rarely detectable at physical examination [16]. Strikingly, half of our patients were asymptomatic, yet imaging revealed a twofold enlargement of the cranial nerve and/or of the skull base foramen in the majority of cases (Table 2 and 3). Our results confirmed non-specific PNS risk factors reported in the literature, including large tumour size, rapid tumour progression, male gender, mid-face location of the tumour, stage T3 or T4 at diagnosis, recurrence after treatment, tumour subtype (SCC, salivary gland tumours), and poor histological differentiation [16]. We found a preponderance of sensory over motor dysfunction (48% sensory symptoms, 41% motor symptoms), which explains patient complaints about pain,
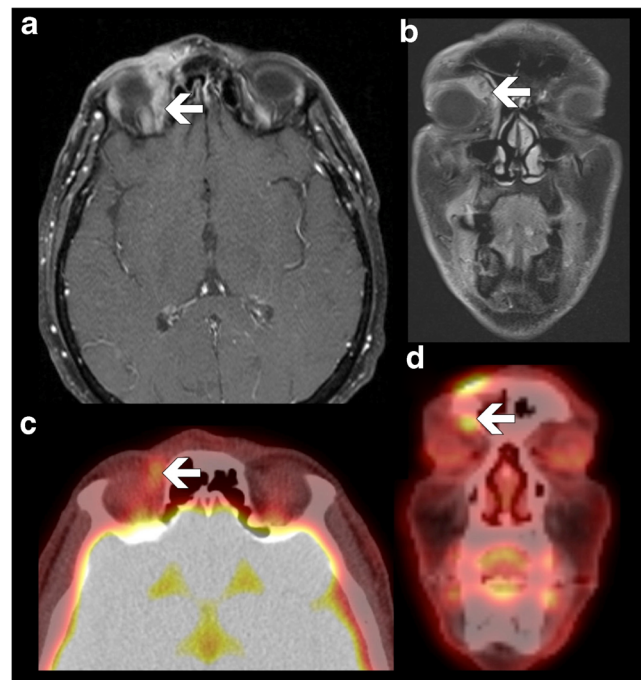

Fig. 4 PNS along cranial nerve V1. T1-weighted sequences with gadolinium chelate (A: axial view, B: coronal view) are compared with 18F-FDG PET/CT (C: axial view, D: coronal view). Increased contrast enhancement (MRI) and increased FDG uptake are associated with a linear enlargement within the distributions of the trigeminal nerve (V^1)

paraesthesia, and numbness, in line with the fact that motor dysfunction usually appears at a later stage [16].

We evaluated whether quantitative imaging biomarkers extracted from PNS were effective in predicting patient overall survival. This was intended to be a proof of concept of the feasibility of PET-guided management strategies for further prospective studies. We demonstrated that the presence or absence of PNS on medical imaging is a binary imaging biomarker associated with poorer overall survival in the population of patients with SCC (*p* = 0.003). The hazard ratio for mortality in patients with PNS was 5.5 in a multivariate analysis including the T-stage, the N-stage, and the M-stage. As a proof of concept, we compared the prognostic value of four quantitative imaging biomarkers: the ratio of cranial nerve diameter, the ratio of foramen diameter, the ratio of cranial nerve SUV_{max}, and the ratio of cranial nerve HISUV. In univariate analysis, we showed that increased glucose consumption was significantly associated with poorer survival (*p* = 0.001). We also explored whether heterogeneity in glucose consumption was associated with a poorer outcome, given that (i) increased glucose metabolism is a hallmark of cancer, and (ii) tumour heterogeneity is associated with poorer outcome and treatment failure because of the generation of resistant phenotypes [24–26]. We hypothesised that the heterogeneity of FDG uptake would differ between PNS and healthy nervous tissue, as demonstrated in peripheral nerve sheath tumours in neurofibromatosis type 1 [19]. Our results

Fig. 5 PNS along cranial nerve V2. An enlargement of the right cranial nerve V^2 is associated with increased FDG uptake (18F-FDG PET/CT: A, B, D) and increased gadolinium enhancement (MRI: C, E). An enlargement of the right foramen rotundum (FR, coronal view: A, B, C) is noted in the skull base. Invasion of the pterygopalatine fossa (PPF) is also observed (axial view: D, E)
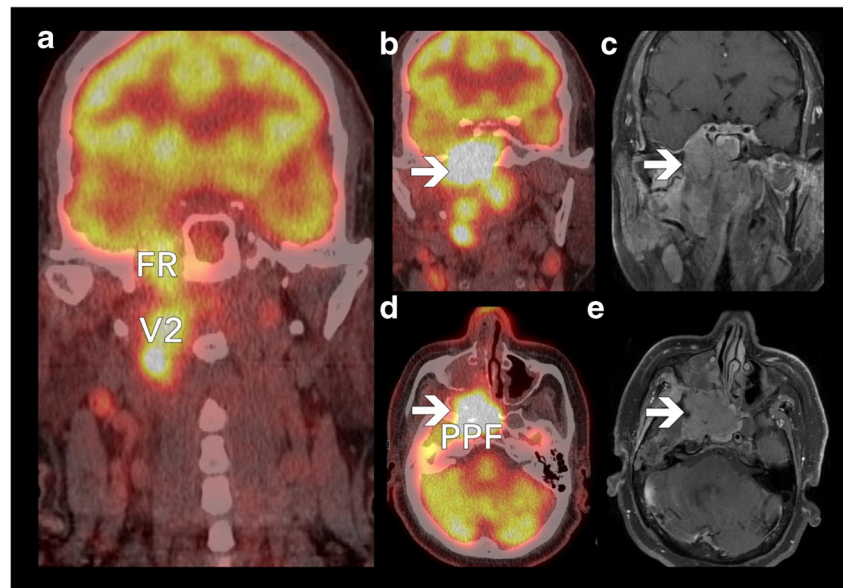
demonstrate that heterogeneity in FDG uptake within the PNS is indeed similar to that of the primary tumour, and is significantly higher than physiological brain uptake. However, the association between HISUV and overall survival did not outperform SUV_{max}, and HISUV may be difficult to standardise among centres, further demonstrating the current limitations of heterogeneity as an imaging biomarker [27].

The detection of PNS is crucial for preoperative evaluation. The goal of surgery will be complete excision of the cranial nerve involved with free margins; skull base surgery is sometimes considered in centres with surgical expertise [28]. MRI is the reference standard for preoperative surgical mapping [23] and for the detection of postoperative complications (e.g. cerebral spinal fluid leak) and incomplete tumour resection. Because of its ability to detect distant metastases, the use of 18F-FDG PET helps avoid unnecessary surgery. In our series, the majority of patients with PNS had locoregional disease (62% N0, 91% M0).

Diagnosis of PNS is critical for radiation therapy planning, as it can change the dose distribution, fractionation, treatment time, and target volume [29–31]. New techniques such as intensity-modulated radiation therapy (IMRT) enable the delivery of an effective radiation dose to the pathological structure, including the entire extent of PNS, while limiting the
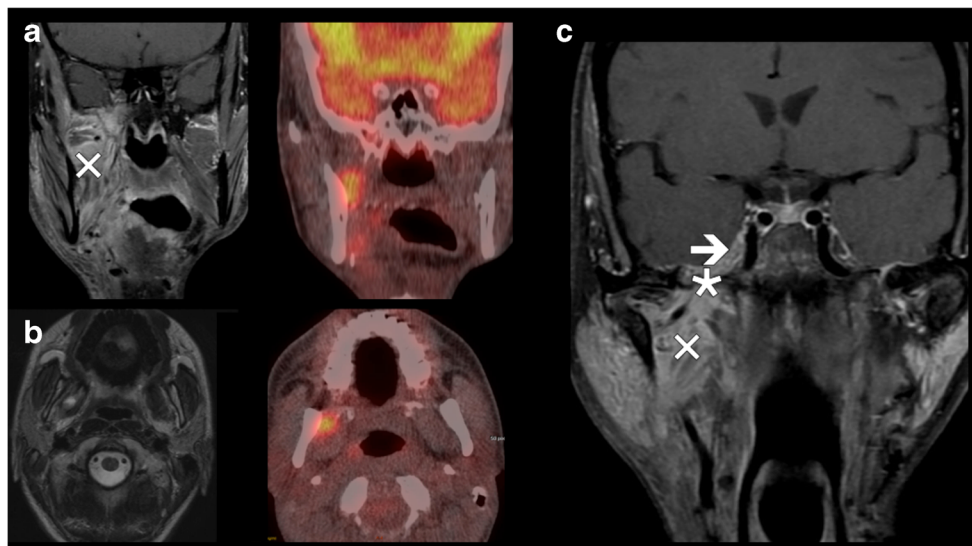

Fig. 6 18F-FDG PET/CT suggested a relapse earlier than MRI. MRI (T1-weighted sequences with gadolinium chelate: A, C; T2-weighted sequence: B) and 18F-FDG PET/CT (A, B) are compared in coronal views (A, C) and axial views (B). MRI and 18F-FDG PET/CT were performed after radiotherapy (A, B) and reassessed 3 months later (C). Initially, the pattern on MRI was not specific: either a scar due to radiotherapy or relapse can cause increased enhancement. It was observed in the cavernous sinus (*arrow*), foramen ovale (*), pterygoid muscle, and infratemporal fossa (x). The association with increased uptake of FDG was suggestive of relapse, which was confirmed at 3 months on MRI

dose to healthy tissue. Based on our series, further prospective studies should investigate whether the combination of F18-FDG PET and MRI findings could help to define optimal tumour volumes for external beam radiation therapy in patients with PNS by (i) guiding the treatment of patients with complex tumour shape or targets close to critical structures, (ii) defining the biological target volume, and (iii) defining the zone for targeting of the boost dose of radiation therapy, since the anatomical location of failure after radiation therapy is most often within the PET biological target volume [32].

The ability to detect PNS by 18F-FDG PET paves the way for further prospective studies investigating PET/CT- or PET/MRI-guided approaches for the early detection of relapse after locoregional treatment. The diagnostic accuracy of MRI is decreased after locoregional treatment because of nonspecific inflammatory contrast enhancement (Fig. 5: focal increased FDG uptake suggesting a relapse on PET; inflammatory scarring after chemoradiation masked the early relapse on MRI, which was subsequently confirmed on MRI 3 months later). MRI can fail to differentiate post-treatment changes from residual/recurrent tumours. In this context, it is important to stress the excellent negative predictive value of post-therapy 18F-FDG PET at 3 months for the evaluation of both the primary tumour and lymph nodes. Consequently, 18F-FDG PET might be of special interest for response evaluation (Fig. 5) by differentiating inflammatory changes (diffuse and homogeneous FDG uptake) from treatment failure (focal increased and heterogeneous uptake).

There are limitations to our study: (i) because of the low frequency of PNS, the study was retrospective in nature and used a case–control design; (ii) the increased demand for glucose due to the Warburg effect is a hallmark of cancer tissue [33] that is non-specific and can be observed in tissue proliferation such as infectious and inflammatory processes [34]; (iii) the reading was very sensitive by a pair of trained imaging specialists; (iv) the number of patients was limited, although this is the largest PNS series on PET to date; and (v) no alpha adjustment was made in this exploratory study.

In conclusion, 18F-FDG PET/CT enabled the detection of PNS in FDG-avid HNM using the direct and indirect signs described above. Precision medicine approaches guided by PET/CT or PET/MR should thus be evaluated in prospective studies for prognostic stratification, delineation of the biological tumour volume prior to external beam radiation therapy, treatment response evaluation, and early diagnosis of relapse in the post-treatment setting.

Compliance with ethical standards

References

1. Trotta BM, Pease CS, Rasamny JJ, Raghavan P, Mukherjee S (2011) Oral cavity and oropharyngeal squamous cell cancer: key imaging findings for staging and treatment planning. RadioGraphics 31:339–354

2. Wahl RL, Jacene H, Kasamon Y, Lodge MA (2009) From RECIST to PERCIST: evolving considerations for PET response criteria in solid tumors. J Nucl Med 50:122S–150S

3. Dercle L, Chisin R, Ammari S et al (2015) Nonsurgical giant cell tumour of the tendon sheath or of the diffuse type: are MRI or 18F-FDG PET/CT able to provide an accurate prediction of long-term outcome? Eur J Nucl Med Mol Imaging 42:397–408

4. Dercle L, Seban RD, Lazarovici J et al (2017) 18F-FDG PET and CT-scan Detect New Imaging Patterns of Response and Progression in Patients with Hodgkin Lymphoma Treated by Anti-PD1 Immune Checkpoint Inhibitor. J Nucl Med. https://doi.org/10.2967/jnumed.117.193011

5. Balink H, de Visscher JG, van der Meij EH (2014) Recurrent head and neck desmoplastic melanoma with perineural spread along the nervus mandibularis revealed by 18F-FDG PET/CT. Int J Oral Maxillofac Surg 43:941–943

6. Paes FM, Singer AD, Checkver AN, Palmquist RA, La Vega GD, Sidani C (2013) Perineural spread in head and neck malignancies: clinical significance and evaluation with 18F-FDG PET/CT. RadioGraphics 33:1717–1736

7. Nguyen BD, Roarke MC (2008) Salivary duct carcinoma with perineural spread to facial canal: F-18 FDG PET/CT detection. Clin Nucl Med 33:925–928

8. Lee TJ, Glastonbury CM, Buckley AF, Eisele DW, Hawkins RA (2008) Perineural spread of melanoma demonstrated by F-18 FDG PET With MRI and pathologic correlation. Clin Nucl Med 33:106–108

9. Conrad GR, Sinha P, Holzhauer M (2004) Perineural spread of skin carcinoma to the base of the skull: detection with FDG PET and CT fusion. Clin Nucl Med 29:717–719

10. Fosko SW, Hu W, Cook TF, Lowe VJ (2003) Positron emission tomography for basal cell carcinoma of the head and neck. Arch Dermatol 139:1141–1146

11. Sekine T, BARBOSA F, Delso G et al (2016) Resectability assessment of head and neck cancer-PET/MR versus PET/CT. J Nucl Med 57:625–625

12. Schaarschmidt BM, Heusch P, Buchbender C et al (2016) Locoregional tumour evaluation of squamous cell carcinoma in the head and neck area: a comparison between MRI, PET/CT and integrated PET/MRI. Eur J Nucl Med Mol Imaging 43:92–102

13. Kuhn FP, Hullner M, Mader CE et al (2014) Contrast-enhanced PET/MR imaging versus contrast-enhanced PET/CT in head and neck cancer: how much MR information is needed? J Nucl Med 55: 551–558

14. Rodrigues RS, Bozza FA, Christian PE et al (2009) Comparison of whole-body PET/CT, dedicated high-resolution head and neck PET/CT, and contrast-enhanced CT in preoperative staging of clinically M0 squamous cell carcinoma of the head and neck. J Nucl Med 50:1205–1213

15. Nemec SF, Herneth AM, Czerny C (2007) Perineural tumor spread in malignant head and neck tumors. Top Magn Reson Imaging 18: 467–471

16. Caldemeyer KS, Mathews VP, Righi PD, Smith RR (1998) Imaging features and clinical significance of perineural spread or extension of head and neck tumors. RadioGraphics 18:97–110 quiz 147

17. Parker GD, Harnsberger HR (1991) Clinical-radiologic issues in perineural tumor spread of malignant diseases of the extracranial head and neck. RadioGraphics 11:383–399

18. Gandhi D, Gujar S, Mukherji SK (2004) Magnetic resonance imaging of perineural spread of head and neck malignancies. Top Magn Reson Imaging 15:79–85

19. Sachpekidis C, Larribere L, Pan L, Haberkorn U, Dimitrakopoulou-Strauss A, Hassel JC (2015) Predictive value of early 18F-FDG PET/CT studies for treatment response evaluation to ipilimumab in metastatic melanoma: preliminary results of an ongoing study. Eur J Nucl Med Mol Imaging 42:386–396

20. Ginsberg LE (1999) Imaging of perineural tumor spread in head and neck cancer. Seminars in Ultrasound, CT and MRI. Elsevier, pp 175-186

21. Nemzek WR, Hecht S, Gandour-Edwards R, Donald P, McKennan K (1998) Perineural spread of head and neck tumors: how accurate is MR imaging? Am J Neuroradiol 19:701–706

22. Caldemeyer KS, Mathews VP, Righi PD, Smith RR (1998) Imaging features and clinical significance of perineural spread or extension of head and neck tumors. RadioGraphics 18:97–110

23. Nemzek WR, Hecht S, Gandour-Edwards R, Donald P, McKennan K (1998) Perineural spread of head and neck tumors: how accurate is MR imaging? AJNR Am J Neuroradiol 19:701–706

24. Ogino S, Stampfer M (2010) Lifestyle factors and microsatellite instability in colorectal cancer: the evolving field of molecular pathological epidemiology. J Natl Cancer Inst 102:365–367

25. Ogino S, Goel A (2008) Molecular classification and correlates in colorectal cancer. J Mol Diagn 10:13–27

26. Ogino S, Chan AT, Fuchs CS, Giovannucci E (2011) Molecular pathological epidemiology of colorectal neoplasia: an emerging transdisciplinary and interdisciplinary field. Gut 60:397–411

27. Dercle L, Ammari S, Bateson M et al (2017) Limits of radiomic-based entropy as a surrogate of tumor heterogeneity: ROI-area, acquisition protocol and tissue site exert substantial influence. Sci Rep 7:7952

28. Dean NR, White HN, Carter DS et al (2010) Outcomes following temporal bone resection. Laryngoscope 120:1516–1522

29. Brahme A (1988) Optimization of stationary and moving beam radiation therapy techniques. Radiother Oncol 12:129–140

30. Yu CX, Tang G (2011) Intensity-modulated arc therapy: principles, technologies and clinical implementation. Phys Med Biol 56:R31–R54

31. Johnston M, Yu E, Kim J (2012) Perineural invasion and spread in head and neck cancer. Expert Rev Anticancer Ther 12:359–371

32. Soto DE, Kessler ML, Piert M, Eisbruch A (2008) Correlation between pretreatment FDG-PET biological target volume and anatomical location of failure after radiation therapy for head and neck cancers. Radiother Oncol 89:13–18

33. Halbrook CJ, Lyssiotis CA (2017) Employing Metabolism to Improve the Diagnosis and Treatment of Pancreatic Cancer. Cancer Cell 31:5–19

34. Vander Heiden MG, Cantley LC, Thompson CB (2009) Understanding the Warburg effect: the metabolic requirements of cell proliferation. Science 324:1029–1033